Int J Appl Earth Obs Geoinformation 74 (2019) 269–280

Contents lists available at ScienceDirect

Int J Appl Earth Obs Geoinformation

journal homepage: www.elsevier.com/locate/jag

A simplified urban-extent algorithm to characterize surface urban heat islands on a global scale and examine vegetation control on their spatiotemporal variability

T. Chakraborty*, X. Lee

School of Forestry & Environmental Studies, Yale University, United States

ARTICLE INFO

Keywords:
Urban heat island
Urban climate
Global study
Remote sensing
MODIS
Algorithm development

ABSTRACT

We develop a new algorithm, the simplified urban-extent (SUE) algorithm, to estimate the surface urban heat island (UHI) intensity at a global scale. We implement the SUE algorithm on the Google Earth Engine platform using Moderate Resolution Imaging Spectroradiometer (MODIS) images to calculate the UHI intensity for over 9500 urban clusters using over 15 years of data, making this one of the most comprehensive characterizations of the surface UHI to date. The results from this algorithm are validated against previous multi-city studies to demonstrate the suitability of the method. The dataset created is then filtered for elevation differentials and percentage of urban area and used to estimate the diurnal, monthly, and long-term variability in the surface UHI in different climate zones. The global mean surface UHI intensity is 0.85 °C during daytime and 0.55 °C at night. Cities in arid climate show distinct diurnal and seasonal patterns, with higher surface UHI during nighttime (compared to daytime) and two peaks throughout the year. The diurnal variability in surface UHI is highest for equatorial climate zone (0.88 °C) and lowest for arid zone (0.53 °C). The seasonality is highest in the snow climate zone and lowest for equatorial climate zone. While investigating the change in the surface UHI over a decade and a half, we find a consistent increase in the daytime surface UHI in the urban clusters of the warm temperate climate zone (0.04 °C/decade) and snow climate zone (0.05 °C/decade). Only arid climate zones show a statistically significant increase in the nighttime surface UHI intensity (0.03 °C/decade). Globally, the change is mainly seen during the daytime (0.03 °C/decade). Finally, the importance of vegetation differential between urban and rural areas on the spatiotemporal variability is examined. Vegetation has a strong control on the seasonal variability of the surface UHI and may also partly control the long-term variability. The complete UHI data are available through this website (https://yceo.yale.edu/research/global-surface-uhi-explorer) and allows the user to query the UHI of urban clusters using a simple interface.

1. Introduction

The urban heat island (UHI) effect refers to the positive temperature difference between an urban area and its hinterland, and it is one of the most well-known consequences of urbanization on local climate (Souch and Grimmond, 2006). It has been an active area of research in urban climatology since it was first observed a century back by Luke Howard (Howard, 1833). Traditionally, it was defined as the air temperature difference between the urban zone and its surroundings, known as the canopy UHI, and was studied using in-situ weather stations or mobile measurements (Voogt, 2007). The advent of satellite data has allowed us to define a new kind of urban heat island, known as the surface UHI, which is the difference in land surface temperature (LST) between the urban area and its surrounding non-urban area (Rao, 1972). Canopy and surface UHI intensities are similar at the annual scale but may have different diurnal and seasonal variabilities (Cui and De Foy, 2012; Chakraborty et al., 2016).

Urbanization changes the surface energy budget by modifying albedo, reducing evaporative cooling via replacement of vegetated surfaces with built-up surfaces, increasing heat storage due to the higher heat capacity of urban structures, and changing dissipation of heat via modulation of thermal roughness and urban spatial configuration (Goward, 1981; Taha, 1997; Arnfield, 2003; Connors et al., 2013; Zhao et al., 2014; Debbage and Shepherd, 2015). For heavily polluted cities in arid regions, dust particles can trap longwave radiation and increase the nighttime UHI intensity (Cao et al., 2016). Other major determinants of the UHI intensity mentioned in the literature are synoptic conditions, city size, precipitation, humidity, cloud cover, and coastal

* Corresponding author.
E-mail address: tc.chakraborty@yale.edu (T. Chakraborty).

https://doi.org/10.1016/j.jag.2018.09.015
Received 10 May 2018; Received in revised form 14 September 2018; Accepted 20 September 2018

feedback (Santamouris, 2015).

Studies quantifying the magnitude of the UHI effect have been performed for hundreds of cities around the world (Oke, 1979; Arnfield, 2003; Santamouris, 2015). Traditionally, such studies are done on a city-by-city basis, which can lead to inconsistencies due to differences in data collection processes, sensor types, and other methodological considerations. A systematic critique of the UHI literature (Stewart, 2011) found that roughly half of the UHI studies lacked robustness. Some important issues were: not controlling for weather factors, lack of information on site metadata and instrumentation, lack of accounting for temporal variability during mobile surveys, inconsistency in defining both urban and rural measurement locations, and disregarding the effect of scale.

The use of satellite data has reduced the inconsistency in measurement techniques by allowing a standardized data collection approach that can be implemented for multiple cities. Previously, Tran et al. (2006) and Imhoff et al. (2010) used satellite data to investigate the surface UHI of 18 Asian megacities and 38 highly populated US cities, respectively. Systematic studies have also been performed on the UHI intensity of cities in Europe (Schwarz et al., 2011; Zhou et al., 2013). A recent study investigated the diurnality and seasonality of the surface UHI in the 84 largest cities in India (Shastri et al., 2017). The principal works done on multiple cities at the global scale are by Peng et al. (2011), who analyzed the UHI of 419 largest cities using 5 years of MODIS AQUA LST data and Clinton and Gong (2013), who investigated the global pattern of the UHI intensity for 2010.

For both canopy and surface UHI studies, one persistent issue is the definition of the rural station (for canopy UHI) or the boundary between the urban and rural area (for surface UHI) (Martin-Vide et al., 2015). Nearby rural areas are affected by advection from the urban core. However, if the rural station is too far away, local weather changes might be more important than the impact of land use changes. A recent study in China found that the footprint of the UHI can be twice or thrice the area of the city (Zhou et al., 2015). This is much higher than the area of the fixed buffer zones normally used in global UHI studies (Clinton and Gong, 2013). The study also demonstrated that for closely located cities, the effect of advection from other cities could also have an impact on the UHI intensity.

Smaller urban areas have generally been overlooked in the existing UHI literature, which disproportionately focuses on large mega-cities. Moreover, the temporal and seasonal variability of the UHI intensity has not been investigated at a global scale. So in this study, we map the daytime and nighttime surface UHI for all urban areas currently detectable via MODIS-based spectral classification of land use using over 15 years of observed data. Buffer-based analyses of the UHI intensity are common in the literature and it is hard to choose a fixed buffer width that is reasonable for all the cities across the globe. So we develop a new algorithm, the simplified urban-extent algorithm (SUE), that can be used to automatically calculate the UHI intensity at a global scale. The algorithm is implemented on Google Earth Engine, a cloud-based platform for planetary-scale data archiving and geospatial analysis (Gorelick et al., 2017). We estimate the surface UHI intensity for almost 9500 distinct urban clusters and estimate the diurnal, seasonal, and annual pattern of the UHI intensity for each climate zone. Many of the factors that influence the UHI intensity, like urban albedo, longwave trapping by the urban canyon, surface roughness, etc. do not show significant seasonal or temporal variations, given the relatively constant nature of urban areas. The main varying characteristic is vegetation cover, which changes throughout the year, as well as between years. Given the focus on the seasonal and temporal variability of the UHI in the present study, we examine how vegetation controls this dynamic globally, and for different climate zones.

The major research questions investigated in the present study are:

- How well does the newly designed SUE algorithm replicate the known characteristics of the surface UHI effect?
- How does the mean, diurnal, and seasonal patterns of the UHI compare for urban clusters in different climate zones?
- How has the UHI intensity changed in the last decade and a half, both globally and for each climate zone?
- How strongly does vegetation control the seasonal and temporal variability of the surface UHI?

Section 2 describes the SUE algorithm developed for this study. Section 3 shows the comparison of the results with those obtained from previous multi-city studies. Section 4 shows the general results as well as the diurnal, seasonal, and annual variability of the surface UHI for urban clusters in different climate zones. Section 5 examines how vegetation controls the spatiotemporal variability of the UHI and discusses the advantages and disadvantages of the SUE algorithm.

2. Methodology

2.1. The Simplified Urban-Extent (SUE) algorithm

In this study, we define the surface UHI as the difference in LST of the urban pixels and the non-urban pixels within each urban extent, which we call the simplified urban-extent (SUE) algorithm. First, the MODIS-derived LST data from TERRA (MOD11A2) and AQUA (MYD11A2) satellites, available at 1 km × 1 km resolution, are preprocessed, with only the clear-sky pixels with average LST error of less than or equal to 3 K being selected for further analysis. The quality controlled datasets are then used to estimate the LST at 0130, 1030, 1330, and 2230 local time (LT). Data from 2000 to 2017 (18 years) are used from the TERRA platform, while data from 2002 to 2017 (16 years) are used from AQUA.

The urban extent data are from Natural Earth (2018). It is a combination of the global urban land database by Schneider et al. (2009, 2010) and the Oak Ridge National Laboratory's LandScan population database (Dobson et al., 2000). The urban data are based on MODIS measurements for February 2001 to February 2002 and is defined using the C4.5 decision tree algorithm (Quinlan, 1993). This dataset has already been validated, with an overall accuracy of 93%, using a Landsat-based map of 140 urban areas in different ecoregions, and for different levels of population and economic development (Schneider et al., 2010). These global urban data are intersected with Thiessen polygons derived from the LandScan population points to create the urban land database; the results are in vector format on the Natural Earth website (2018). The urban units are closed polygons around contiguous urban agglomerations. Fig. 1 shows an example of one such urban unit consisting of multiple urban areas. The advantage of using this dataset is that it is based on a consistent algorithm implemented on the MODIS land use satellite product and bounds the global hot spots of human habitation.

Fig. 1 shows the steps used to estimate the surface UHI of each urban cluster. Firstly, the global LST and MODIS LU/LC data (at 500 m × 500 m resolution) for 2013 (MCD12Q1) are clipped to the urban extent dataset. Then, two subsets are created, one for urban land use (in red in Fig. 1) and another for all land use other than urban and water based on the land use data. The water pixels are removed since the high specific heat capacity of water would lead to an overestimation of the UHI intensity during the daytime and an underestimation during nighttime. After subsetting, the spatial mean of the LST for both subsets are calculated for each urban cluster and their difference is the surface UHI for that cluster. Before taking the spatial means, the subsetted LST pixels are automatically resampled to 500 m × 500 m grids to match the resolution of the LU/LC data. When calculating the surface UHI for separate years, the same extent shape is applied to all years, though the subsetting is done using the MODIS LU/LC data for that particular year. Since the MODIS LU/LC data are only available till 2013, the 2013 data are also used for the years 2014–2017. Unless otherwise stated, the daytime UHI is derived from the mean of LST values at 1030 and 1330

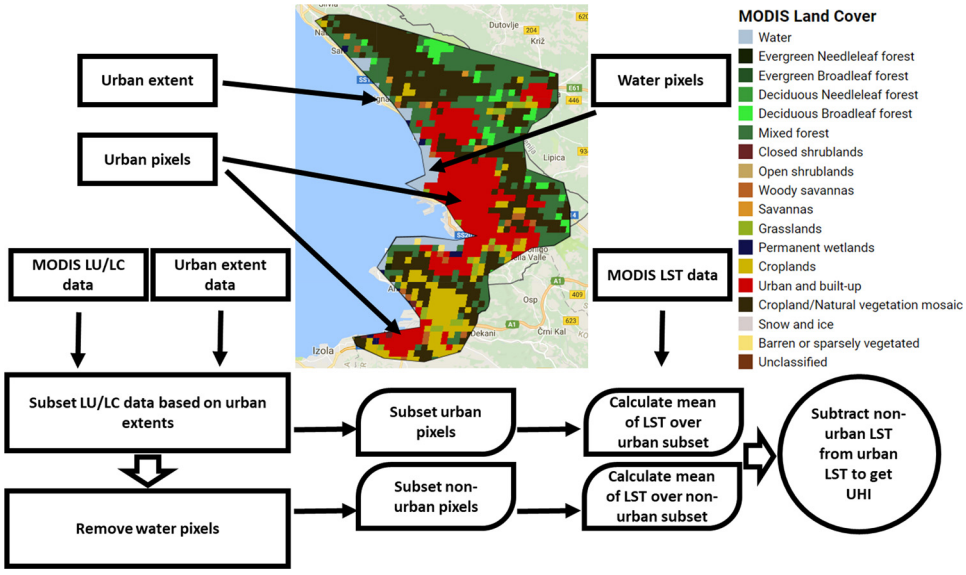

Fig. 1. Sequence of steps used to estimate the surface UHI for each urban cluster. First, a subset of the MODIS LU/LC data are created based on the urban extent dataset. Two subsets of these data are created; one for urban land use, and another for non-urban, non-water land use. The mean of the LST over these LU/LC pixels gives the urban and rural temperatures, respectively. Finally, the difference between these two is the calculated surface UHI. The figure also shows one example of urban units used in the present study, along with the MODIS LU/LC dataset used to create the subsets.

LT, while the nighttime UHI is based on the mean of the LST at 0130 and 2230 LT. The same method is used to find the difference in Enhanced Vegetation Index (EVI) (ΔEVI), a proxy for green vegetation density, between the urban and rural pixels using the AQUA 16-day EVI dataset available at 250 m × 250 m resolution (MYD13Q1) for the same time period.

Evidently, the algorithm, in its current form, does not work for the clusters that are entirely urban or rural. This is especially true for small clusters (with area < 3 km^2) with very few pixels. We remove the clusters with no rural pixels. After removing these from the original dataset of 12022 separate clusters, we are left with 9483 urban clusters. Since the difference in elevation between the urban and rural pixels can influence the UHI intensity, the dataset was further filtered to only include those clusters with a mean elevation difference of less than 50 m. For this, we use the Global Multi-resolution Terrain Elevation Data 2010 (GMTED2010), which combines terrain elevation data from multiple sources and is available at 7 arc seconds (roughly 30 m at the equator) (Danielson and Gesch, 2011). Finally, to further constrain the variability in the ratio of urban to rural pixels for each cluster, only the clusters with at least 10% urban area are considered. The surface UHI is then calculated using all the available data after quality control (from 2000 to 2017 for TERRA and from 2002 to 2017 for AQUA). For the summer surface UHI, data for June, July, and August are considered for the Northern Hemisphere and December, January and February for the Southern Hemisphere. For winter, June, July, and August are considered for the Southern Hemisphere and December, January and February for the Northern Hemisphere. The final dataset consists of 7374 urban clusters comprising 760,600 km^2 with 38.78% of the total area (294,960 km^2) being urban with a mean elevation difference of 4.46 m between urban and rural pixels. This is similar to the area analyzed by Clinton and Gong (2013), though we use a new algorithm and 16 years of data versus the one year (2010) used in that study. The multiple years of data allow us to characterize the long-term variability of the surface UHI and get better uncertainty estimates of the seasonal trend and annual values.

2.2. Latitudinal pattern of the surface UHI

The zonal characteristics of the UHI at a global scale are first investigated. To do this, the Earth is divided into 5-degree latitudinal increments and the mean and standard error of the UHI intensity are computed for each increment. Some urban clusters lie on the boundary between two latitudinal increments and this would lead to double counting. To avoid this, the centroid of each urban cluster is determined before grouping into the latitudinal increments. Peng et al. (2011) characterized the latitudinal variability of the surface UHI difference between summer and winter using MODIS AQUA data for the 419 largest cities. For the purpose of algorithm validation, this is also done with the 419 largest urban clusters in the present study (Section 3).

2.3. Climatic variability of the surface UHI

While zonal characteristics can give an overview of the global surface UHI characteristics, it cannot account for any forcing other than the latitudinally varying incoming solar radiation. There is some evidence that the surface UHI intensity is influenced by the background climate of the city (Zhao et al., 2014). Zonal characterization cannot account for differences in background climate since there may be multiple climate zones in one latitudinal increment. Thus, in the present study, the surface UHI characteristics are separately investigated for each climate zone.

The updated Koppen–Geiger classification data for 1901–2100 are used, based on the Rubel and Kottek (2010). The Koppen–Geiger classification divides the world into 5 major climate zones: equatorial, arid, warm temperate, snow, and polar (Fig. S1(a)). Similar to the latitudinal classification, the centroids of the urban clusters are used for grouping to minimize double counting using an XY tolerance of 500 m on ArcMap. There are 762 urban clusters in the equatorial climate zone, 1136 in the arid climate zone, 3968 in the warm temperate climate zone, 1499 in the snow climate zone. The latitudinal variation of the urban clusters for each climate zone is in Fig. S1(b), the distribution of the area of urban clusters is in Fig. S2, and the distribution of the percentage of urban pixels in each cluster is in Fig. S3. All the urban clusters in the polar climate zone are filtered out since the elevation difference between the rural and urban pixels is > 50 m in all these clusters. The total number of urban clusters in all climate zone, when added, is 7374, which is 9 less than the total number of clusters in the global dataset. This is because the climate zone vector used in the grouping process do not enclose the position of some of the urban centroids. In addition, several urban clusters are double counted as they are in two or more climate zones at once; a result of the XY tolerance used while grouping. Since the sample size is large, these small discrepancies are trivial.

Table 1
Summary of surface UHI characteristics (mean ± standard deviation) for the largest 419 urban clusters compared to the largest 419 cities considered by Peng et al. (2011).

Source	TERRA (present study)	AQUA (present study)	Peng et al.
Annual day (°C)	1.11 ± 1.05	1.50 ± 1.26	1.50 ± 1.20
Annual night (°C)	0.89 ± 0.44	0.80 ± 0.44	1.10 ± 0.50
Summer day (°C)	1.62 ± 1.47	2.03 ± 1.64	1.90 ± 1.50
Summer night (°C)	1.05 ± 0.45	0.90 ± 0.41	1.00 ± 0.05
Winter day (°C)	0.64 ± 0.77	0.96 ± 1.00	1.10 ± 1.20
Winter night (°C)	0.86 ± 0.61	0.78 ± 0.61	1.00 ± 0.70

3. Validation of results

Peng et al. (2011) used the city-clustering algorithm by Rozenfeld et al. (2008) to define the urban areas at a fine scale. Then, they estimated the surface UHI as the difference in LST between the city core and its rural hinterland using MODIS AQUA data. In contrast, the SUE algorithm developed in the present study uses the difference in the mean LST of the urban pixels and the mean LST of the non-urban pixels within the same urban extent to define the surface UHI. To validate the accuracy of SUE at estimating the surface UHI versus the method used by Peng et al. (2011), the surface UHI intensities from AQUA for the 419 largest urban clusters in the dataset (same as the number of cities studied by Peng et al. (2011) were calculated. The surface UHI intensities for TERRA were also calculated for comparison. The daytime and nighttime surface UHI intensities (mean ± standard deviation) for annual, summer and winter for both methods are shown in Table 1. The results from the SUE algorithm are in line with the results from the city-clustering algorithm, especially for daytime. During nighttime, the SUE algorithm slightly underestimates the surface UHI (around 27% underestimation for annual nighttime surface UHI), while wintertime UHI intensity is biased low for both daytime and nighttime.

The study by Peng et al. (2011) did not show any major seasonality for the nighttime surface UHI, with annual, wintertime and summertime mean values being very close. On the contrary, the present study shows that the summertime UHI is the highest and the wintertime UHI is the lowest, and the annual mean UHI is between those two values. This is consistent with the observations for the 419 largest cities derived from the TERRA dataset. The seasonality of the UHI is discussed in more detail in Section 4.

The slight deviation from the previous values may not only be due to the different methodologies. The present study uses 16 years (from 2002 to 2017) of data for AQUA compared to 6 years of data (from 2003 to 2008) used in Peng et al. (2011). Moreover, the largest 419 urban clusters are not same as the largest 419 cities. Many of the larger urban clusters are created from contiguous cities. Thus, the 419 largest urban clusters incorporate more area than the 419 largest cities used in Peng et al. (2011). Moreover, in the present study, MODIS pixels with an error greater than 3 K are removed before the final analyses.

The latitudinal variation of the AQUA-derived surface UHI differences between summer and winter for the 419 largest urban clusters is compared with the pattern seen from the methodology used by Peng et al. (2011) in Fig. S4. The study by Peng et al. (2011) used 15 latitudinal increments to find the variation, whereas we use 20 latitudinal increments of 5-degree width. Overall, both methods show very similar patterns. For daytime, the values from the present study have a less pronounced latitudinal variability. Otherwise, the peaks and troughs are roughly replicated by our methodology. The only exception is the opposite trend seen for 20 degrees South latitude. For nighttime, the patterns from the two algorithms are even more similar in magnitude and latitudinal variability.

Clinton and Gong (2013) also calculated the surface UHI for all global urban areas for 2010 using 5 - and 10-km buffers. We compared the 2010 data from the present study with the results of that study (Table 2). The UHI values found here are very similar to the values calculated using 5-km buffers and lower than those calculated using 10-km buffers. The standard deviations of the UHI values are lower in the present study.

Table 2
Summary of surface UHI characteristics (mean ± standard deviation) for the all urban areas compared to the results from Clinton and Gong (2013)

Local time	Present study (SUE)	Clinton and Gong (5-km buffer)	Clinton and Gong (10 km buffer)
0130 LT	0.51 ± 0.47	0.60 ± 0.90	0.70 ± 1.00
1030 LT	0.73 ± 0.86	0.70 ± 1.40	1.00 ± 1.60
1330 LT	1.00 ± 1.08	0.90 ± 1.60	1.10 ± 1.80
2230 LT	0.60 ± 0.47	0.60 ± 0.90	0.80 ± 1.00

The results of present study are in agreement with the results of the buffer-based analysis for large cities and all cities. Thus, we are confident that the SUE algorithm is a viable alternative to buffer-based characterizations of surface UHI intensity.

4. Results

4.1. Global patterns

Fig. 2 shows the global map of the mean surface UHI for daytime and nighttime derived from MODIS satellite measurements. The global mean surface UHI intensity is 0.85 °C for daytime and 0.55 °C for nighttime. The majority (87%) of the urban clusters show a positive daytime surface UHI, with 44% showing values greater than 1.00 °C. During nighttime, 93% of the urban clusters show positive UHI intensities, but only 13% show value greater than 1.00 °C. The urban clusters with negative surface UHI are concentrated in the dry and desert areas, namely the Arabian Desert in the Middle East, the Chihuahuan Desert in southern US and Mexico, the Thar Desert along the border of India and Pakistan, the Kalahari Desert in southern Africa, and the Patagonian Desert in the southern part of South America. The nighttime surface UHI intensities are generally lower than the daytime values. Daytime UHI is influenced by more factors like the difference in evaporative cooling and surface roughness between urban and rural areas, anthropogenic heat flux, and thermal inertia of built-up structures (Zhao et al., 2014). In contrast, nighttime UHI is primarily influenced by heat storage from the daytime, and anthropogenic heat flux. This explains why the temperature differential is higher during the day than at night.

When the UHI derived from AQUA and TERRA are analyzed separately, the data from AQUA shows higher values during daytime and lower values during nighttime. Table 3 summarizes the surface UHI intensity from the global dataset from both TERRA and AQUA platforms. The annual daytime surface UHI intensity is greater than the nighttime intensity for both TERRA and AQUA. The daytime and nighttime summer surface UHI intensities are larger than their corresponding winter time components. The daytime intensity for summer are over twice the UHI intensity for winter for both TERRA and AQUA. For nighttime, the seasonal difference is less pronounced. The daytime surface UHI is larger than the nighttime surface UHI for all cases. Paired *t*-tests were performed between all daytime and nighttime datasets and they were found to be statistically significant with $p < 0.01$ for all cases.

4.2. Latitudinal patterns

Fig. 3 shows the latitudinal variation in the surface UHI for daytime and nighttime. The solid lines show the mean surface UHI intensities for each 5-degree latitudinal increments, while the shaded portions

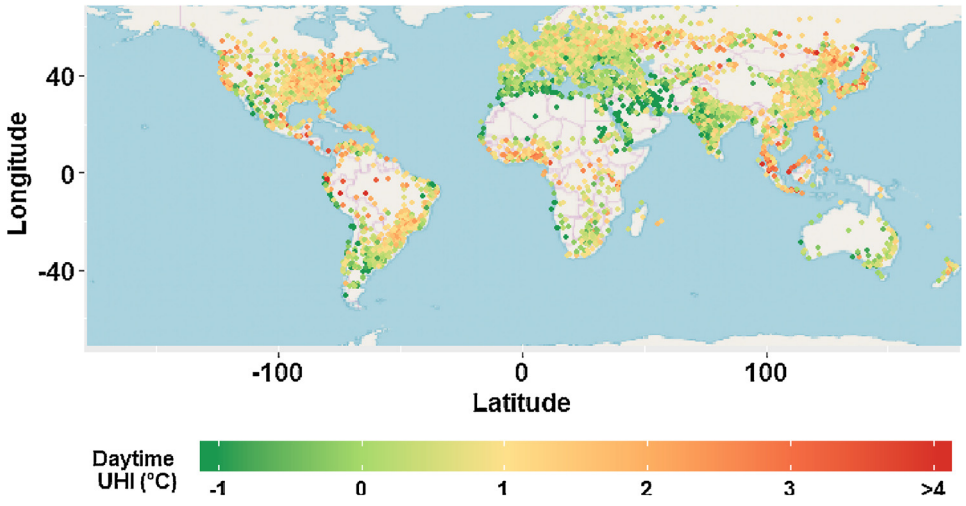

(a) Daytime

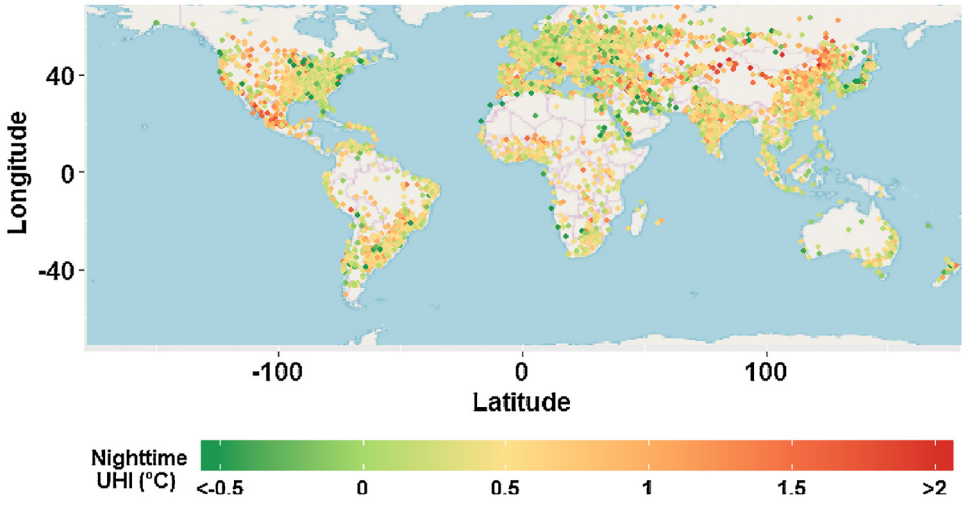

(b) Nighttime

Fig. 2. Global map of mean surface UHI for 7374 urban clusters estimated using the SUE algorithm. The daytime value is the mean of the UHI intensity at 1030 LT derived from TERRA (2001–2017) and the UHI intensity at 1330 LT derived from AQUA (2003–2017). The nighttime value is the mean of the UHI intensity at 2230 LT derived from TERRA and the UHI intensity at 0130 LT derived from AQUA.

represent the standard error from the mean. The daytime and nighttime surface UHI intensities show distinct patterns. For daytime, there are pronounced positive surface UHI intensities around the equator, at 20 degrees South, and between 40 and 60 degrees North. Compared to the daytime UHI, the nighttime UHI shows lesser latitudinal variability. There is a pronounced nighttime UHI at 30 degrees North and around 10 degrees South. At around 25 degrees North and 30 degrees South, the daytime and nighttime UHI intensities flip, i.e. the nighttime

Table 3
Summary of global surface UHI characteristics, where the sample size is 7374. Differences in daytime and nighttime UHI intensities are statistically significant ($p < 0.01$) for all cases.

Period	Local time	Mean	Standard deviation	1st quartile	2nd quartile	3rd quartile
Annual	0130 LT	0.51	0.44	0.25	0.50	0.75
	1030 LT	0.71	0.82	0.30	0.74	1.17
	1330 LT	1.00	1.04	0.44	1.02	1.59
	2230 LT	0.59	0.44	0.32	0.56	0.84
Summer	0130 LT	0.57	0.44	0.30	0.55	0.82
	1030 LT	1.12	1.19	0.45	1.18	1.87
	1330 LT	1.44	1.42	0.61	1.51	2.36
	2230 LT	0.69	0.46	0.40	0.67	0.96
Winter	0130 LT	0.50	0.54	0.19	0.44	0.75
	1030 LT	0.35	0.59	0.09	0.35	0.63
	1330 LT	0.53	0.79	0.13	0.52	0.92
	2230 LT	0.57	0.54	0.24	0.50	0.84

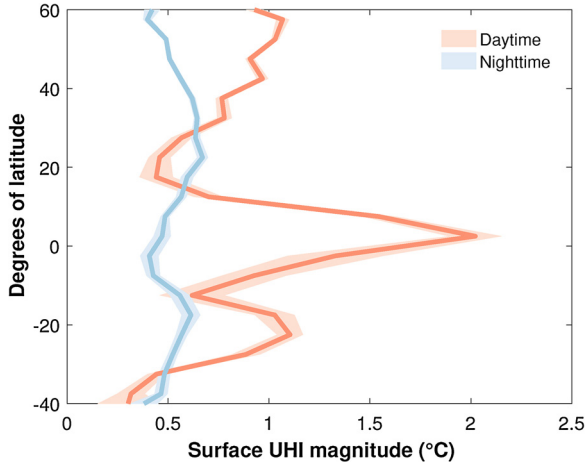

Fig. 3. Latitudinal variation in surface UHI intensity. The solid lines are for mean values, while the shaded portions represent the standard error. The daytime and nighttime intensities are consolidated values from TERRA and AQUA platforms.

surface UHI is greater than the daytime intensity. These latitudes are predominantly arid and cities in arid climate show higher nighttime surface UHI intensity (refer Section 4.3). This reversal of the UHI diurnality in desert cities has been observed in previous studies (Imhoff et al., 2010; Zhang et al., 2010; Lazzarini et al., 2013).

4.3. Variations across climate zones

Fig. 4 shows the mean and standard error of the daytime and nighttime surface UHI categorized into the Koppen–Geiger climate zones. For daytime, the highest surface UHI is for the equatorial urban clusters, followed by snow, warm temperate, and arid. Arid urban clusters, in particular, have nearly zero daytime UHI. This pattern is consistent at both 1030 LT and at 1330 LT. For nighttime, arid urban clusters have the highest UHI intensity. The urban clusters in equatorial, warm temperate and snow climate zones all show very similar surface UHI intensities. The daytime surface UHI is greater than the nighttime surface UHI for all climate zones other than the arid. Paired *t*-tests confirm that the difference between the daytime and nighttime UHI intensity is statistically significant ($p < 0.01$) for all climate zones.

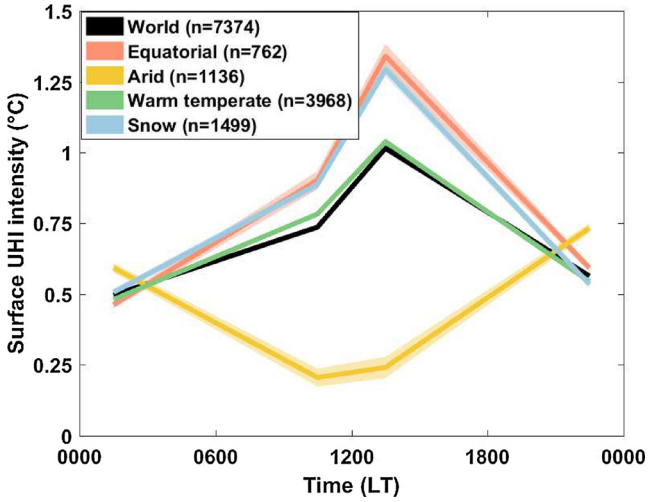

Fig. 5. Diurnality of the surface UHI for the world and each climate zone. The solid lines represent the mean value, while the shaded areas represent the standard errors.

4.4. Diurnality

The daytime and nighttime measurements from TERRA and AQUA were combined to calculate the diurnality of the surface UHI intensity for the world and for each climate zone. In Fig. 5, the solid lines represent the mean of the diurnal variation, while the shaded regions show the one standard error from the mean. As discussed previously, globally, the surface UHI intensity is higher during the day than at night, which has been seen in previous studies (Peng et al., 2011; Clinton and Gong, 2013). The present study shows that this diurnality is consistent across all the climate zones except the arid zone. Among equatorial, warm temperate, and snow urban clusters, the UHI intensity is highest at 1330 LT and lowest at 0130 LT. For the arid zone, the highest surface UHI intensity is at 2230 LT and the lowest is at 1030 LT.

The diurnal range of the surface UHI – the difference between the maximum and minimum surface UHI intensities – is highest for the equatorial urban clusters (0.88 °C), followed by 0.79 °C for snow, 0.56 °C for warm temperate, and 0.53 °C for arid. Overall, the diurnal range of the surface UHI is 0.52 °C. The standard error of UHI intensity is very low because of the large sample size.

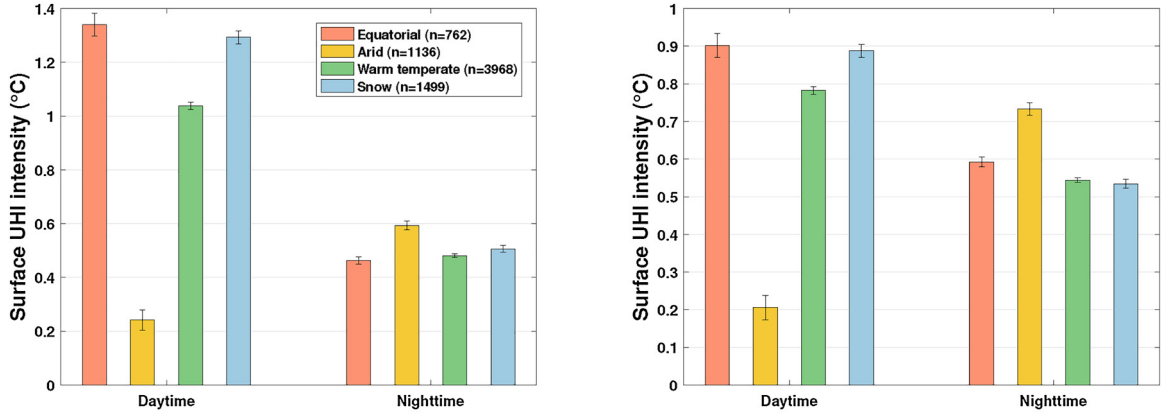

Fig. 4. Global daytime and nighttime surface UHI intensities (mean ± standard error) for each climate zone.

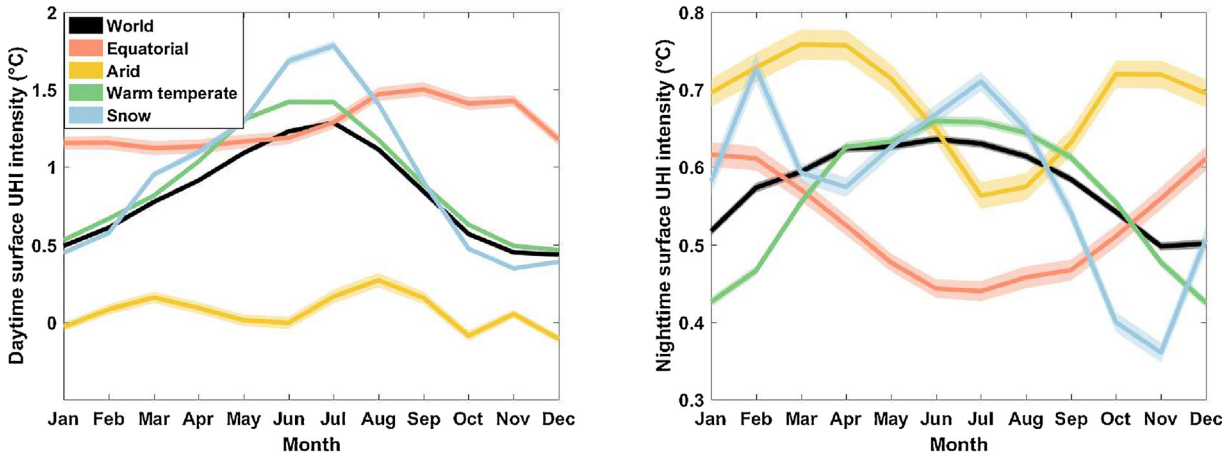

Fig. 6. Seasonal variability in global daytime and nighttime surface UHI intensities for each climate zone. The solid lines represent the mean value, while the shaded areas represent the standard errors.

4.5. Seasonal variability

The monthly means and standard errors of the surface UHI intensity for each of the 12 months of the year are presented in Fig. 6. Globally, the daytime surface UHI shows higher values during the boreal summer, with the highest intensities in July (1.29 ± 0.01 °C) and the lowest values in December 0.43 ± 0.01°C.

When the data are divided into climate zones, all of them do not show the same pattern. The warm temperate and snow urban clusters show comparable patterns with low values during the boreal winter and high values during boreal summer. For daytime, the maximum surface UHI intensities for the warm temperate and snow urban clusters are during the boreal summer (1.43 ± 0.02 °C in June for warm temperate; 1.78 ± 0.03 °C in July for snow) and the lowest values are in boreal autumn (0.46 ± 0.01 °C in December for warm temperate; 0.35 ± 0.01 in November °C for snow). The daytime surface UHI intensity in the equatorial and arid zones show distinct patterns. For the arid urban clusters, there is hardly any seasonality compared to the other climate zones. Moreover, the daytime surface UHI intensities are close to zero for most of the year. The daytime surface UHI in the equatorial climate zone shows the opposite pattern to the warm temperate and snow climate zones, with the highest values during boreal autumn and the lowest values during boreal spring.

The seasonality of the global nighttime surface UHI is similar to the daytime pattern with June highs and November lows (Fig. 6 (b)). The nighttime surface UHI of the warm temperate climate zone shows high values during boreal summer (July) and low values in boreal autumn (December). Like the daytime case, the seasonality of the monthly surface UHI is atypical for equatorial and arid zone. The arid zone again shows two peaks during the year, one in March and another in October. The minimum surface UHI in the arid urban clusters is in July. The equatorial zone shows the highest surface UHI intensity in boreal winter (January) and the minimum in boreal summer (July). For nighttime, urban clusters in the snow climate zone also show two peaks during the year, one in February and another in July. The lowest nighttime intensity for this climate zone is in November.

The maximum daytime surface UHI intensity in all climate zones other than equatorial are in and around boreal summer. Eighty-nine percent of the urban clusters considered in the present study are in the Northern Hemisphere. Moreover, most of the urban clusters in the Southern Hemisphere are in the Tropics, which show very little seasonality. Since the energy imbalance due to urban land use (due to changes in albedo, thermal mass, evapotranspiration, etc.) is a function of the magnitude of incoming solar radiation, it makes sense that the surface UHI is highest when the Northern Hemisphere receives the highest net radiation. When the dataset is separated into hemispheres, the seasonal variation is identical in the Northern Hemisphere and reverses for the Southern Hemisphere (Fig. S5). For the Southern Hemisphere, the peak daytime surface UHI intensity is shifted towards the austral summer for all the climate zones. Nighttime surface UHI shows very little seasonal variation in the Southern Hemisphere.

The global inter-seasonal range of the daytime UHI – the difference between the maximum and minimum mean monthly daytime surface UHI intensities during the 12-month cycle – is 0.85 °C. The highest seasonality in the daytime surface UHI is 1.44 °C for urban clusters in the snow climate zone, followed by warm temperate zone (0.95 °C). Inter-seasonal range of daytime surface UHI 0.38 °C for both equatorial and arid climate zone. The inter-seasonal range of the global nighttime UHI is very low (0.14 °C). A recent multi-city study showed that many urban centers in India show a negative surface UHI during daytime during the hot period (Shastri et al., 2017). This dampens the seasonality of the daytime UHI in the equatorial climate zone. The snow urban clusters show the highest inter-seasonal range of nighttime UHI intensity (0.37 °C), followed by warm temperate (0.23 °C), arid (0.19 °C), and equatorial (0.18 °C).

Very few studies have investigated the seasonality of the UHI on a month-by-month basis for multiple cities (Debbage and Shepherd, 2015). Clinton and Gong (2013) looked at the time of maximum and minimum surface UHI intensity for cities around the globe, though they did it only for 2010. This is the first study to characterize the seasonality of the surface UHI at a global scale using all available MODIS observations.

4.6. Long-term trend

Fig. 7 shows the temporal variability in the annual UHI from 2003 to 2017 based on aggregated data from TERRA and AQUA. The change per decade for each case, along with its 95% confidence interval, is mentioned in the figure. Globally, the daytime surface UHI shows a positive temporal trend, with an increase of around 0.03 ± 0.02°C per decade. In comparison, the nighttime surface UHI intensities have remained practically unchanged (−0.00 ± 0.01°C per decade). The increase in the daytime UHI intensity is highest for the snow urban clusters (0.05 ± 0.03°C per decade) and lowest in the arid zone (−0.03 ± 0.01°C per decade).

For nighttime, the surface UHI intensity does not show any significant change (with 95% confidence), except for urban clusters in the arid zone, which show an increasing trend (0.03 ± 0.01°C per decade). Daytime surface UHI intensity has decreased significantly in arid urban clusters over the last decade and a half. This makes sense because urban clusters in arid climate are cooler than their surroundings (Zhao et al., 2014) and expansion of these areas over time would intensify these

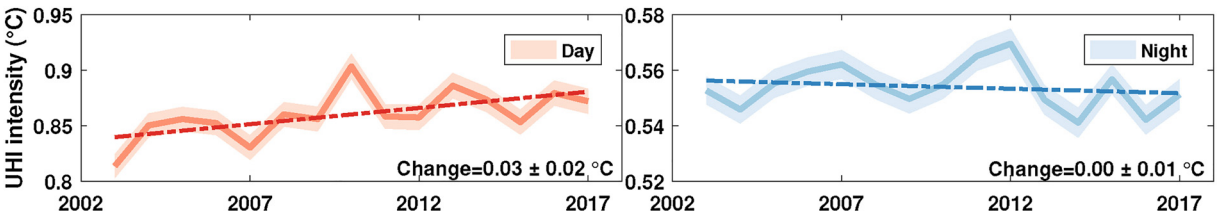

(a) World

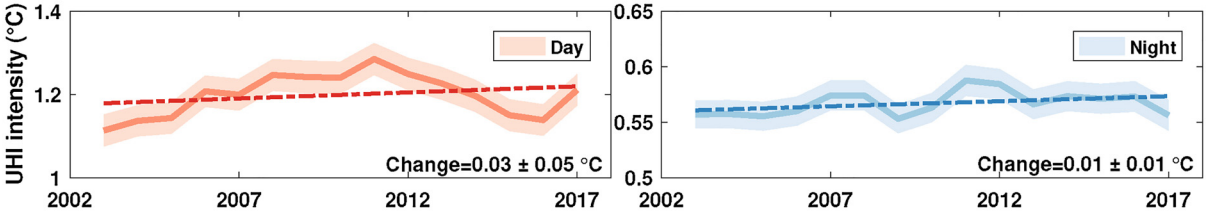

(b) Equatorial climate zone

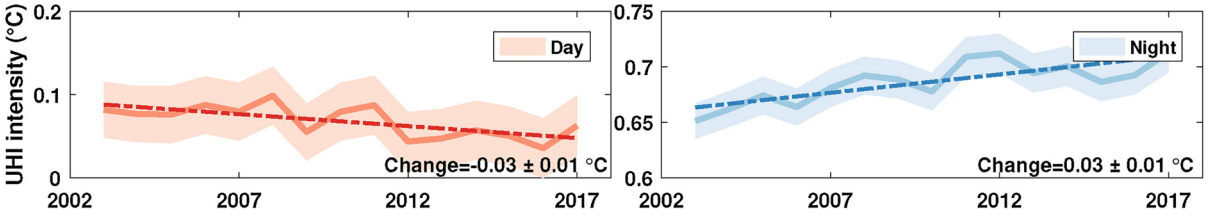

(c) Arid climate zone

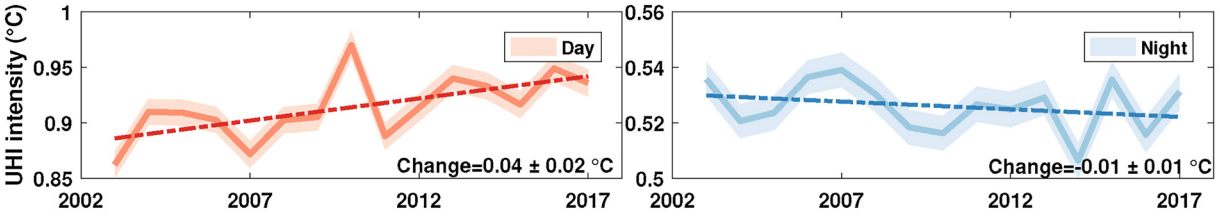

(d) Warm temperate climate zone

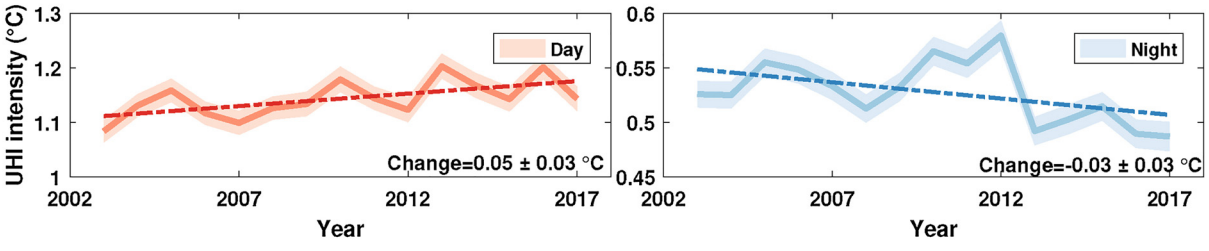

(e) Snow climate zone

Fig. 7. Temporal variability in annual daytime and nighttime surface UHI intensities from 2003 to 2017. The solid lines represent the mean values, while the shaded areas represent the standard errors. The dashed line represents the trend for best linear fit and the change in the surface UHI intensity per decade (mean ± 95% confidence interval) is mentioned on each plot.

urban cool islands. The daytime UHI intensity change over the warm temperate zone, which includes the majority of urban clusters in Europe and North America, is also positive. The present study is the first investigation of how the surface UHI has changed over the last decade and a half on a global scale and for each climate zone using observed data.

In comparison to the changes found here, the global land temperature anomalies have increased at the rate of 0.30°C per decade from 2003 to 2017 (NOAA, 2018). It should be noted that since the surface UHI is calculated in reference to non-urban land use, the changes in UHI intensity found in the present study is in addition to the increase in surface temperature due to global climate change. In comparison,

deforestation shows a much stronger effect, though the strength and sign of change depend on the latitude (Lee et al., 2011). A recent study using MODIS LST products from 2003 to 2013 found an increase in average surface temperature at the rate of 0.28°C per decade in equatorial regions, a maximum cooling of 0.55 °C per decade in boreal regions, and a warming of up to 0.32 °C per decade in temperate regions (Li et al., 2016).

Previously, two such studies (Fischer et al., 2012; Oleson, 2012) have analyzed the difference in urban and rural response to climate change using global climate models, i.e. the change in the UHI intensity. Depending on the climate change scenario used (best to worst), the UHI either stayed the same or slightly reduced compared to the present day scenario. However, these studies did not take urban expansion into consideration, which could be influencing the changes observed in the present study.

5. Discussion

5.1. Vegetation control on the surface UHI intensity

Several previous studies have shown that difference in vegetation between the urban and rural areas strongly modulates the surface UHI intensity via differential evaporative cooling of urban versus rural surfaces. This has been seen when comparing surface UHI of multiple cities (Peng et al., 2011; Clinton and Gong, 2013), as well as when comparing the seasonal surface UHI trend of individual cities (Qiao et al., 2013; Chakraborty et al., 2016). Similarly, in the present study, when the dataset is divided into increasing ΔEVI quartiles, the daytime surface UHI intensity decreases (Fig. 8). This is particularly true for global, equatorial, arid, and warm temperate cases. For the snow urban clusters, daytime surface UHI increases slightly for the highest ΔEVI bin. This is because these cities are primarily in the northern latitudes, where vegetation control is less dominant. Similarly, there is no consistent association between nighttime UHI and ΔEVI since, mechanistically, impact of vegetation on surface temperature is dominant during daytime.

We examine how the seasonality of the ΔEVI modulates the seasonal variability of the surface UHI. The monthly ΔEVI accounts for 95% of the variance in the monthly daytime UHI at a global scale (Fig. 9). Similar strong correlations are found for urban clusters in warm temperate ($r^2 = 0.94$) and snow ($r^2 = 0.84$) climate zones. The correlations are not statistically significant ($p > 0.01$) for urban clusters in equatorial and arid zones. This is partly because the seasonal variability is lowest in these climate zones as they are nearer to the equator. Moreover, vegetation is not a strong determinant of the daytime UHI in the arid zone and the equatorial region is strongly influenced by other factors, like cloudiness, monsoonal rainfall, etc, which can impact the UHI intensity.

The rural EVI shows a stronger seasonal cycle than the urban EVI for all climate zones other than equatorial, which modulates the differential evaporative cooling between urban and rural areas, and thus, the daytime UHI intensity (Fig. S6). The nighttime surface UHI shows a much weaker association with the ΔEVI, suggesting that it is not strongly controlled by the vegetation differential between urban and rural surfaces, as also found in a previous study (Peng et al., 2011). For nighttime, the association is only statistically significant for the world and warm temperate climate zones (Fig. S7).

Similar correlations were attempted between the yearly daytime and nighttime surface UHI intensities and the yearly ΔEVI values (Figs. S8 and S9). The relationships are much weaker, except for the arid zone. Temporal analyses of the urban and rural EVI over 16 years show that the rate of change of urban EVI per decade is lower than the corresponding change in the rural EVI (Fig. S10). Globally, the urban EVI has remained the same while the rural EVI has increased slightly. However, these results are near the detection limit of MODIS.

5.2. Advantages of the SUE algorithm

One major advantage of the SUE algorithm is that it can be automated to estimate the surface UHI intensity at a global scale. We do not need to explicitly define a buffer around an urban area to implement this algorithm. Instead, we use the urban boundaries as the units of calculation, with the spectral classification of remotely sensed data being used to separate the urban and rural pixels. The choice of a buffer around an urban area can be arbitrary. Moreover, studies on individual cities sometimes use administrative boundaries to define the urban area, which are usually not related to the physical characteristics of urban land use. In comparison, the rural area in the Natural Earth dataset used in this iteration of the SUE algorithm is the non-built-up pixels of human-inhabited regions of Earth. Thus, the surface UHI, as defined in this study, is the temperature change experienced by people as they move into built-up areas.

Since the footprint of the UHI varies significantly and can be up to 3.9 times the city area for nighttime, the choice of the rural pixel can significantly affect the calculated UHI intensity (Zhou et al., 2015). In many cities, especially developing cities, the city is surrounded by satellite towns with their own urban influence. This lack of standardization of the urban and rural area in the context of the UHI effect was also pointed out by Stewart and Oke (Stewart and Oke, 2009). The SUE algorithm, as implemented in this study, merges many of these satellite towns by using urban clusters, which is one step towards standardization.

5.3. Limitations of the study

While the SUE algorithm, as used in this study, solves a few methodological issues in the existing UHI literature, it has limitations mainly due to the datasets used in the present study. The urban extent database used in the present study is based on satellite observations from 2001 to 2002. Urban areas have grown since then, especially Asian and African cities, which have experienced tremendous urban sprawl in the last decade. The urban pixels of the MODIS MCD12Q1 raster data have also remained same since 2002 (Li et al., 2017). In addition, due to the nature of the urban extent data used in the study, some MODIS urban pixels transcend the urban extents, leading to a reduction of urban data points for some clusters. Given the large number of data points, this does not cause widespread biases at the global or regional scale. Since we do not use explicit buffers around the urban areas, the rural reference sprawls in an anisotropic manner, which could create biases in the estimated surface UHI for individual cities. Buffer-based estimates of surface UHI of coastal cities have the same problem, with the data from the buffer over the water pixels not being used as a part of the rural reference. In addition to the anisotropy in the rural reference, the percentage of urban clusters within each pixel varies significantly (Fig. S3), from 10% to roughly 98%. Caution should be exercised when comparing the surface UHI of individual clusters because of this disparity in the percentage of the urban area between different clusters.

These are mostly issues with the datasets used, not the SUE algorithm itself. New, more recent urban datasets, if available, can be used in conjunction with the SUE algorithm to create updated maps of the surface UHI.

While MODIS data products are relatively accurate over homogeneous terrain, their accuracy decreases substantially over heterogeneous surfaces, for instance, urban areas. To control for this, we have only considered the pixels with less than 3 K uncertainty. We initially tried using only pixels with an uncertainty of less than 1 K. However, doing so removes the majority of urban pixels. It should be noted that this uncertainty is an issue with all satellite-based observations of UHI intensity.

In addition to the uncertainty of the urban pixels, the MODIS thermal band used for LST retrieval is constrained to clear sky conditions. The impact of cloud contaminated pixels could significantly alter

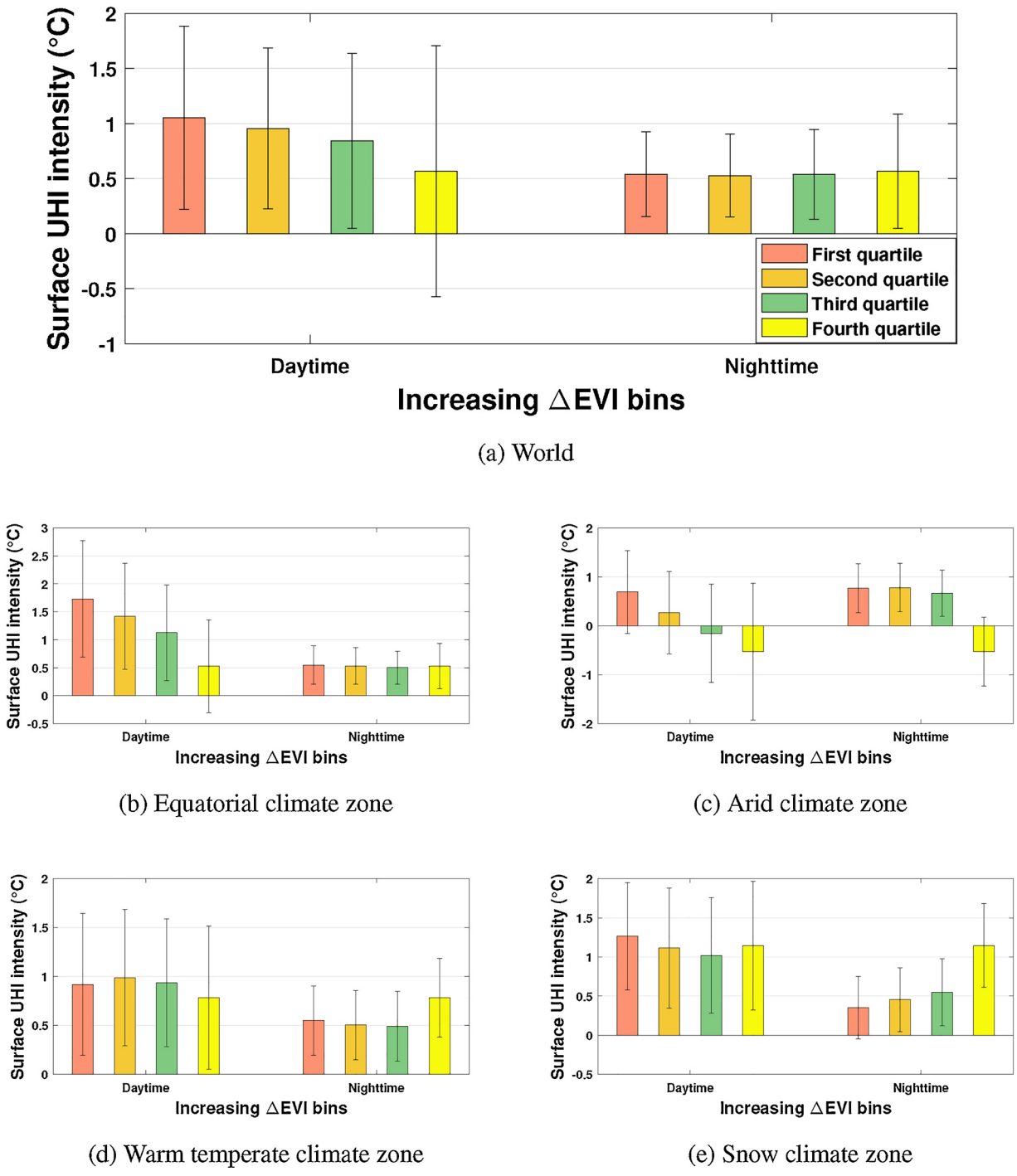

Fig. 8. Daytime and nighttime surface UHI intensity (mean ± standard deviation) for increasing urban–rural EVI difference bins.

the estimated UHI intensity. While we have considered only clear sky pixels in our calculations, the frequency of cloudy pixels is a function of season and may impact our estimates of the UHI intensity due to biases in sampling. It is important to keep these uncertainties in mind while interpreting the results of this study.

6. Conclusions

A new algorithm (SUE) is designed to study the surface UHI at a global scale. The study validates a few well-known surface UHI characteristics, like latitudinal variability and the annual, summertime, and wintertime intensity. The algorithm extends the analysis by using a complete urban extent dataset and all available MODIS satellite observations. Most important is the analysis of multiple years of data to reduce uncertainties in surface UHI estimates and investigating the long-term variability of the surface UHI.

Globally, the daytime surface UHI is higher than the nighttime UHI, with the summer season showing the highest values compared to winter. The urban extent dataset is divided into climate zones using the Koppen–Geiger climate classification system to investigate the differences in the diurnal, seasonal, and long-term variability in the surface UHI for the first time using a consistent methodology. All climate zones other than arid show higher daytime surface UHI intensities, with snow urban clusters showing the highest diurnal range and maximum

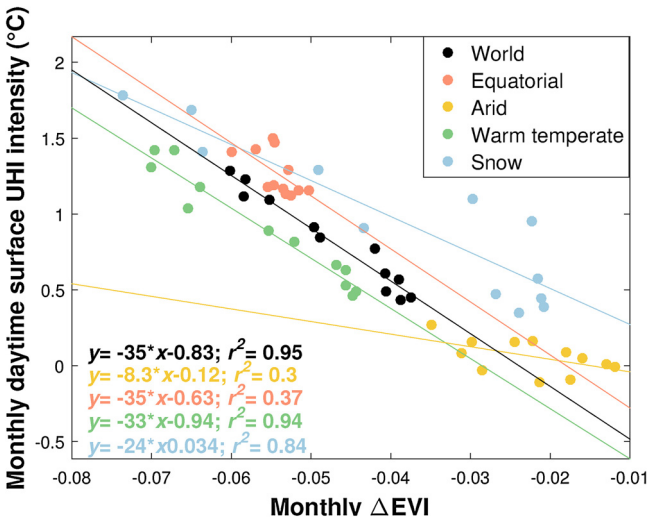

Fig. 9. Association between monthly daytime surface UHI intensity and monthly ΔEVI for all urban clusters, and urban clusters in each climate zone.

daytime values. There are significant differences in the seasonality of the surface UHI for different climate zones, in particular for arid and equatorial urban clusters. The long-term variability in the surface UHI is investigated using yearly land use classes from MODIS. A consistent increase is seen in the surface UHI intensity for urban clusters, particularly for daytime, indicating a temporal redistribution of heat due to urbanization.

Finally, we investigate the importance of vegetation in controlling the surface UHI intensity. Vegetation is a strong modulator of the seasonal variability of the surface UHI, and may also affect the long-term changes observed in this study. Since the difference in vegetation between the urban and rural area is a strong predictor of the surface UHI intensity, increased urban vegetation can be used to dampen UHI intensity in cities prone to heat stress. In particular, seasonal urban irrigation has the potential to mitigate high UHI during the hot season.

This study demonstrates that the urban clusters in different background climates show distinct diurnal, seasonal, and long-term variability using a globally consistent dataset for the first time. Our results indicate that background climate should be taken into consideration for city-specific UHI mitigation policies, as well as when planning new cities and expanding existing urban areas.

7. Data availability

The dataset developed in the present study can be found at (Chakraborty and Lee, 2018). To make the data more accessible, we have also designed an interactive, public facing web application to query urban heat island intensities of almost all urban clusters on the Google Earth Engine platform. It can be accessed here: Global Surface UHI Explorer (https://yceo.yale.edu/research/global-surface-uhi-explorer).

Acknowledgements

We acknowledge Yale Institute for Biospheric Studies (YIBS) for financial support. We thank Prof. Dana Tomlin for his suggestions on the Google Earth Engine script. We also thank two anonymous reviewers whose comments helped us improve this manuscript.

References

Arnfield, A.J., 2003. Two decades of urban climate research: a review of turbulence, exchanges of energy and water, and the urban heat island. Int. J. Climatol. 23 (1), 1–26.

Cao, C., Lee, X., Liu, S., Schultz, N., Xiao, W., Zhang, M., Zhao, L., 2016. Urban heat islands in china enhanced by haze pollution. Nat. Commun. 7.

Chakraborty, T., Lee, X., 2018. Global UHI data table. Dataset on Mendeley. https://doi.org/10.17632/h9pfd42fv9.1#file-9cb9f20e-b16e-4b1f-914e-bbb12cf29916.

Chakraborty, T., Sarangi, C., Tripathi, S.N., 2016. Understanding diurnality and inter-seasonality of a sub-tropical urban heat island. Boundary-Layer Meteorol. 1–23.

Clinton, N., Gong, P., 2013. Modis detected surface urban heat islands and sinks: Global locations and controls. Remote Sens. Environ. 134, 294–304.

Connors, J.P., Galletti, C.S., Chow, W.T., 2013. Landscape configuration and urban heat island effects: assessing the relationship between landscape characteristics and land surface temperature in phoenix, arizona. Landsc. Ecol. 28 (2), 271–283.

Cui, Y.Y., De Foy, B., 2012. Seasonal variations of the urban heat island at the surface and the near-surface and reductions due to urban vegetation in Mexico city. J. Appl. Meteorol. Climatol. 51 (5), 855–868.

Danielson, J.J., Gesch, D.B., 2011. Global Multi-resolution Terrain Elevation Data 2010 (gmted2010), Tech. rep. US Geological Survey.

Debbage, N., Shepherd, J.M., 2015. The urban heat island effect and city contiguity. Comput. Environ. Urban Syst. 54, 181–194.

Dobson, J.E., Bright, E.A., Coleman, P.R., Durfee, R.C., Worley, B.A., 2000. Landscan: a global population database for estimating populations at risk. Photogrammetric Eng. Remote Sens. 66 (7), 849–857.

Fischer, E., Oleson, K., Lawrence, D., 2012. Contrasting urban and rural heat stress responses to climate change. Geophys. Res. Lett. 39 (3).

Gorelick, N., Hancher, M., Dixon, M., Ilyushchenko, S., Thau, D., Moore, R., 2017. Google Earth Engine: Planetary-scale geospatial analysis for everyone. Remote Sens. Environ. 202, 18–27.

Goward, S.N., 1981. Thermal behavior of urban landscapes and the urban heat island. Phys. Geogr. 2 (1), 19–33.

Howard L. (1833) The climate of London: deduced from meteorological observations made in the metropolis and at various places around it, vol 2. Harvey and Darton, J. and A. Arch, Longman, Hatchard, S. Highley [and] R. Hunter.

Imhoff, M.L., Zhang, P., Wolfe, R.E., Bounoua, L., 2010. Remote sensing of the urban heat island effect across biomes in the continental usa. Remote Sens. Environ. 114 (3), 504–513.

Kelso, Nathaniel Vaughn and Patterson, Tom (2018) Urban areas: Cultural vector (1:10m). http://www.naturalearthdata.com/downloads/10m-cultural-vectors/10m-urban-area/.

Lazzarini, M., Marpu, P.R., Ghedira, H., 2013. Temperature-land cover interactions: the inversion of urban heat island phenomenon in desert city areas. Remote Sens. Environ. 130, 136–152.

Lee, X., Goulden, M.L., Hollinger, D.Y., Barr, A., Black, T.A., Bohrer, G., Bracho, R., Drake, B., Goldstein, A., Gu, L., et al., 2011. Observed increase in local cooling effect of deforestation at higher latitudes. Nature 479 (7373), 384–387.

Li, X., Messina, J.P., Moore, N.J., Fan, P., Shortridge, A.M., 2017. Modis land cover uncertainty in regional climate simulations. Clim. Dynam. 49 (11-12), 4047–4059.

Li, Y., Zhao, M., Mildrexler, D.J., Motesharrei, S., Mu, Q., Kalnay, E., Zhao, F., Li, S., Wang, K., 2016. Potential and actual impacts of deforestation and afforestation on land surface temperature. J. Geophys. Res. Atmos.

Martin-Vide, J., Sarricolea, P., Moreno-García, M.C., 2015. On the definition of urban heat island intensity: the "rural" reference. Front. Earth Sci. 3, 24.

NOAA (2018) NOAA national centers for environmental information, climate at a glance: Global time series URL http://www.ncdc.noaa.gov/cag/.

Oke TR. (1979) Review of urban climatology, 1973-1976. 539, Secretariat of the World Meteorological Organization Geneva.

Oleson, K., 2012. Contrasts between urban and rural climate in ccsm4 cmip5 climate change scenarios. J. Clim. 25 (5), 1390–1412.

Peng, S., Piao, S., Ciais, P., Friedlingstein, P., Ottle, C., Bre?on, F.M., Nan, H., Zhou, L., Myneni, R.B., 2011. Surface urban heat island across 419 global big cities. Environ. Sci. Technol 46 (2), 696–703.

Qiao, Z., Tian, G., Xiao, L., 2013. Diurnal and seasonal impacts of urbanization on the urban thermal environment: a case study of Beijing using MODIS data. ISPRS J. Photogrammet. Remote Sens. 85, 93–101.

Quinlan J. (1993) C4. 5: Programs for machine learning. c4. 5-programs for machine learning/j. ross quinlan.

Rao, P.K., 1972. Remote sensing of urban heat islands from an environmental satellite. Bull. Am. Meteorol. Soc. 53 (7), 647.

Rozenfeld, H.D., Rybski, D., Andrade, J.S., Batty, M., Stanley, H.E., Makse, H.A., 2008. Laws of population growth. Proc. Natl. Acad. Sci. 105 (48), 18 702-18,707.

Rubel, F., Kottek, M., 2010. Observed and projected climate shifts 1901–2100 depicted by world maps of the köppen-geiger climate classification. Meteorologische Zeitschrift 19 (2), 135–141.

Santamouris, M., 2015. Analyzing the heat island magnitude and characteristics in one hundred Asian and Australian cities and regions. Sci. Total Environ. 512, 582–598.

Schneider, A., Friedl, M.A., Potere, D., 2009. A new map of global urban extent from modis satellite data. Environ. Res. Lett. 4 (4), 044 003.

Schneider, A., Friedl, M.A., Potere, D., 2010. Mapping global urban areas using modis 500-m data: New methods and datasets based on 'urban ecoregions'. Remote Sens. Environ. 114 (8), 1733–1746.

Schwarz, N., Lautenbach, S., Seppelt, R., 2011. Exploring indicators for quantifying surface urban heat islands of european cities with modis land surface temperatures. Remote Sens. Environ. 115 (12), 3175–3186.

Shastri, H., Barik, B., Ghosh, S., Venkataraman, C., Sadavarte, P., 2017. Flip flop of day-night and summer-winter surface urban heat island intensity in india. Sci. Rep. 7, 40 178.

Souch, C., Grimmond, S., 2006. Applied climatology: urban climate. Progr. Phys. Geogr. 30 (2), 270–279.

Stewart, I., Oke, T., 2009. A new classification system for urban climate sites. Bull. Am. Meteorol. Soc. 90 (7), 922–923.
Stewart, I.D., 2011. A systematic review and scientific critique of methodology in modern urban heat island literature. Int. J. Climatol. 31 (2), 200–217.
Taha, H., 1997. Urban climates and heat islands: albedo, evapotranspiration, and anthropogenic heat. Energy Build. 25 (2), 99–103.
Tran, H., Uchihama, D., Ochi, S., Yasuoka, Y., 2006. Assessment with satellite data of the urban heat island effects in Asian mega cities. Int. J. Appl. Earth Observ. Geoinform. 8 (1), 34–48.
Voogt, J., 2007. How researchers measure urban heat islands. In: In: United States Environmental Protection Agency (EPA), State and Local Climate and Energy Program. Heat Island Effect, Urban Heat Island Webcasts and Conference Calls.
Zhang, P., Imhoff, M.L., Wolfe, R.E., Bounoua, L., 2010. Characterizing urban heat islands of global settlements using MODIS and nighttime lights products. Can. J. Remote Sens. 36 (3), 185–196.
Zhao, L., Lee, X., Smith, R.B., Oleson, K., 2014. Strong contributions of local background climate to urban heat islands. Nature 511 (7508), 216–219.
Zhou, B., Rybski, D., Kropp, J., 2013. On the statistics of urban heat island intensity. Geophys. Res. Lett. 40 (20), 5486–5491.
Zhou, D., Zhao, S., Zhang, L., Sun, G., Liu, Y., 2015. The footprint of urban heat island effect in China. Sci. Rep. 5, 11 160.